Fuel-Rich Natural Gas Conversion in HCCI Engines with Ozone and Dimethyl Ether as Ignition Promoters: A Kinetic and Exergetic Analysis

Dominik Freund, Christoph Horn, and Burak Atakan(✉)

Institute for Combustion and Gas Dynamics (IVG), Chair of Thermodynamics, University of Duisburg-Essen, Lotharstraße 1, D-47057 Duisburg, Germany
burak.atakan@uni-due.de

Abstract. Fuel-rich operated HCCI engines are suitable for the polygeneration of work, heat, and base chemicals like synthesis gas ($CO + H_2$). Under favorable conditions, these engines are exergetically more efficient than separate steam reformer and cogeneration gas engines. However, to achieve ignition, reactive fuel additives like dimethyl ether or ozone must be supplied, which have some, probably negative and not yet quantified, impacts on the exergetic efficiency.

Therefore, the aim of this work is to compute and evaluate the effect of DME and ozone on the exergy input and exergetic efficiency of fuel-rich operated HCCI engines, which convert natural gas at equivalence ratios of 1.5 to 2.5.

Results of a single-zone-model (SZM) and a multi-zone model (MZM) are compared to analyze the influence of inhomogeneities in the cylinder on the system's exergetic efficiency. Natural gas as fuel is compared with previous neat methane results.

The single-zone model results show that natural gas is much more reactive than methane. Ethane and propane convert partially in the compression stroke and lead to ethene, propene, and OH radicals. However, the ethane and propane conversions do not favor but slightly reduce the formation of methyl hydroperoxide, which is an important buffer molecule for fuel-rich methane ignition. But in addition, further buffer molecules like ethene or ethyl hydroperoxide are intermediately formed. The product selectivities are neither influenced by the natural gas composition, nor by the chosen additive.

Compared to ozone, the DME molar and mass fractions needed for ignition are up to 11 times higher, and its exergy contribution to the total mixture is even 95 times higher. Therefore, the system's exergetic efficiency is much higher when ozone is chosen as additive: reasonable values of up to 82.8% are possible, compared to 67.7% with DME. The multi-zone model results show that the efficiency is strongly dependent on the fuel conversion and thus unconverted fuel should be recycled within the polygeneration system to maintain high efficiencies. Comparing the total exergetic efficiency, ozone is a favorable additive for fuel-rich operated HCCI polygeneration.

Keywords: HCCI engines · Polygeneration · Ozone · Dimethyl ether · Partial oxidation

R. King and D. Peitsch (Eds.): AFCC 2021, NNFM 152, pp. 47–65, 2022.
https://doi.org/10.1007/978-3-030-90727-3_4

1 Introduction

Fossil resource usage can be reduced by more efficient and flexible energy and chemical compound conversion technologies. A promising approach is the polygeneration of work, heat, and synthesis gas in fuel-rich operated internal combustion (IC) engines which is a mid-term alternative to separate cogeneration gas engines and steam reforming processes.

Several works in the 2000s and 2010s showed that partial oxidation of methane or natural gas is feasible in spark-ignition (SI), compression ignition (CI), and homogeneous charge compression ignition (HCCI) engines. Each ignition type has its own challenges for stable operation, though.

CI engines typically need an additional fuel injection, e.g. diesel or n-heptane, leading to stratification within the cylinder. Karim et al. [1] investigated the partial oxidation of methane with highly oxygenated air in a dual-fuel CI engine experimentally in 2008 for equivalence ratios of 2.0 to 3.5 and found that this process is feasible and yields up to 80% synthesis gas in the dry exhaust gas. However, a diesel injection was still needed for ignition and combustion control.

Ignition in SI engines is dependent on the flame speed and thus limited to lower equivalence ratios. However, Lim et al. [2] modified a CI engine to perform spark ignition and achieved stable operation of methane/air-mixtures for equivalence ratios up to 2. For ignition, high intake temperatures of up to 450 °C were needed and the spark ignition timing was adjusted between 45 and 30° crank angle (°CA) before top dead center. This operation range could be extended by adding 5% hydrogen and 10% ethane to the fuel mixture – to represent natural gas. Then, a stable operation at an equivalence ratio (ϕ) of up to 2.8 was possible.

A very high flexibility can be achieved with HCCI engines, which are kinetically controlled and thus do not depend on fuel injection timing or flame speed. Our previous experimental work has shown that polygeneration with methane fueled HCCI engines is feasible and exergetic efficiencies of up to 81.5% are achieved [3, 4]. However, methane containing fuels (such as biogas or natural gas) represent a challenge for achieving HCCI due to their inertness leading to high octane-numbers and relatively high specific heat capacities. Ignition can be promoted with reactive additives such as ethers [3] or higher alkanes [5]. In our previous work we found that high additive mass fractions of up to 28% in the fuel mixture are needed when dimethyl ether (DME) [3, 6], diethyl ether (DEE), or n-heptane [4] are used.

The production of these additives leads to additional, yet partially unknown, exergy losses, and the added DME is typically produced from synthesis gas, and thus, is a product of the polygeneration system. Therefore, from a holistic viewpoint, alternatives are preferable. Ozone may be a much more suitable additive, since it is produced on demand via corona discharge [7] using surrounding air and much smaller amounts are needed to ignite methane (typically, less than 5000 ppm). Keum et al. [8] investigated the effect of ozone as an ignition promoter under stoichiometric conditions in 2018 and found that 100 ppm ozone provide a significant promotion effect in HCCI engines, whereas SI engines benefit from an increased flame speed only from an addition of 3000 to 6000 ppm. Sayyosouk et al. [9] modelled a zero-dimensional HCCI engine fueled

with iso-octane at lean conditions ($\phi = 0.3$) and found that even 4 ppm ozone promote ignition effectively.

These results encouraged us to investigate the effect of ozone in fuel-rich operated HCCI engines [10]. There, the influence of ozone on the kinetics of methane in fuel-rich HCCI engines has been investigated in comparison to DME [10]. We have found that ozone is a much more effective additive than DME. Ozone decomposes very early in the compression stroke, does not noticeably increase the heat capacity of the mixture, and it leads to the formation of methyl hydroperoxide (CH_3OOH), which leads to OH radical formation near the end of the compression stroke via formaldehyde (CH_2O) and hydrogen peroxide (H_2O_2) formation. For a practical application, the HCCI engine is likely fueled with natural gas instead of neat methane. Therefore, in the present work the kinetic investigation is extended towards natural gas.

As discussed before, Lim et al. found that the addition of hydrogen and ethane extended the operation stability of fuel rich operated SI engines from $\phi = 2$ to $\phi = 2.8$. Duan et al. [11] compared neat methane with natural gas experimentally in a fuel lean operated HCCI engine. With 2.88% ethane and 0.41% propane in the natural gas mixture, the in-cylinder pressure increased by up to 4 bar, compared to neat methane. Although the combustion phasing (CA50) was shifted slightly towards earlier crank angles, this effect was not significant. Kaczmarek et al. [12] measured ignition delay times of natural gas/DME/air mixtures in a shock tube at fuel rich mixtures ($\phi = 2$, 10) and concluded that under those conditions, natural gas is much more reactive compared to methane due to its ethane and propane contents (which were set to 9% and 1%, respectively). As the natural gas composition may vary during the operation of a fuel-rich HCCI engine, the evaluation of the effect of ozone on the ignition is analyzed here and compared to the operation with neat methane.

Additionally, a comparison between ozone and DME, based on exergy methods, is carried out here. This comparison includes a comparative modelling study on the influence of DME and ozone on the engine's exergy input and their influences on the exergetic efficiency of the polygeneration system. The exergetic efficiency of the ozone generator is calculated with a Python model and the exergetic efficiency of the DME production is taken from the work of Zhang et al. [13]. Zhang et al. conducted a profound exergy analysis on the steam gasification of biomass and determined an exergetic efficiency of 43.5%.

This paper aims to answer the question. whether ozone is an exergetically favorable additive compared to DME, representative for other oxygenated hydrocarbons, when natural gas fueled HCCI engine are operated at equivalence ratios of 1.5 to 2.5. Our previous work [10] showed that trends are well reproduced with a single zone model, while the fuel conversion is overestimated for fuel-rich conditions. Thus, a comparison with a multi-zone model is included here, and the importance of the colder zones on the outcome is analyzed.

2 Methodology

The engine model is written in Python and the thermodynamics and reaction kinetics are computed by using the module Cantera [14]. A four-stroke single-zone model (SZM)

and recently a two-stroke multi-zone model (MZM) were developed. The multi-zone model contains seven zones (numbered as subscript i) with inter-zonal heat and mass transfer and a non-reactive crevice zone of 1.5 vol-% of the dead volume. The heat transfer between the zones $\dot{q}_{i-1\rightarrow i}$ Eq. (1) is modelled as heat conduction according to the approach of Komninos et al. [15], which was developed for HCCI engines [16].

$$\dot{q}_{i-1\rightarrow i} = -k_{tot}\frac{\partial T}{\partial r_n} \cong -k_{tot}\frac{T_i - T_{i-1}}{(t_i + t_{i-1})/2} \tag{1}$$

The temperature gradient $\frac{\partial T}{\partial r_n}$ between two zones is discretized to a temperature difference, whereas $-k_{tot}$, T_i, and t_i are denoted as the total thermal conductivity, the zone temperature, and the zone thickness, respectively. The total thermal conductivity consists of a laminar and a turbulent part, which are calculated by estimating laminar and turbulent Prandtl numbers and gas mixture viscosities. Kominos et al. adapted this approach from Yang and Martin [17] and described it in more detail in [15, 16].

To assure a uniform pressure within all zones, each zone is connected to its adjacent zones within Cantera as valves, allowing a pressure difference dependent mass flow from one zone to another. The crevice zone and the outermost zone also transfer heat and mass to their adjacent zones, but also to the cylinder wall as a global heat transfer. The gas mixture in each zone of the single-zone and the multi-zone model is homogeneous and the piston movement induces volume changes.

For each timestep, the energy and species conservation equations are solved. For the single-zone model, the global heat transfer coefficient is calculated with the semi-empirical Woschni correlation [18] and the coefficients are taken from our recent work [10]. For the multi-zone model, a slightly modified version of the Woschni equation was used, according to Chang et al. [19], who measured the in-cylinder heat fluxes in an HCCI engine experimentally.

Our multi-zone model was then validated against our own measurements with methane/DME mixtures at $\phi = 1.9$ from [10] by using a zone distribution which led to a good agreement between the simulated fuel conversion, work, and heat output and the experimental data.

At TDC, the core zone and the crevice zone are set at 30% and 1.5% of the dead volume, respectively. The remaining volume is distributed between the five other zones so that the volume decreases from the inner to the outermost zone. The bore d and the height of the dead volume h_{TDC} of the cylinder are thus divided into the thickness of the outer zones t_i and the thickness of the core zone $t_{core,x}$ Eq. (2) and $t_{core,y}$, respectively Eq. (3).

$$d = 2\sum t_i + 2t_{core,x} \tag{2}$$

$$h_{TDC} = 2\sum t_i + 2t_{core,y} \tag{3}$$

The core zone thickness in direction of the piston movement $t_{core,y}$ is given by the cylinder height at top dead center h_{TDC} and the sum of the thickness of the outer zones Eq. (4). The thickness $t_{core,x}$ corresponds to the half diameter of the core zone and is kept constant.

$$t_{core,y} = \frac{h_{TDC} - 2\sum t_i}{2} \tag{4}$$

The thickness t_i of each outer zone is calculated according to Eq. (5).

$$t_i = L \bullet R^{N-(i+1)} \tag{5}$$

Here, $N = 7$ is the number of zones, R is set to 0.45 and L is solved within the model to assure that Eq. (3) is fulfilled. The zone volumes change with height changes due to the piston movement. The resulting volume distribution is visualized in Fig. 1.

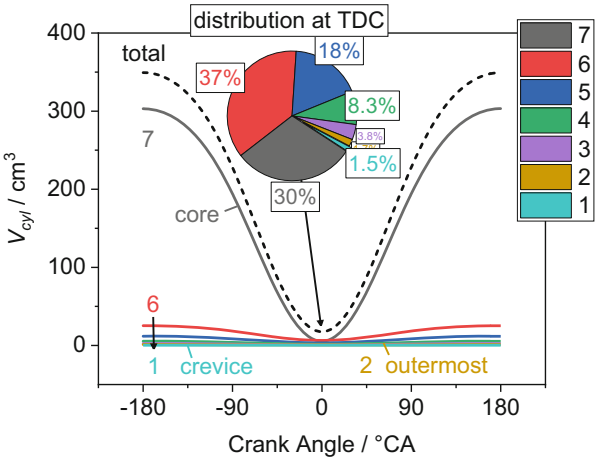

Fig. 1. Volumes of the seven zones of the multi-zone model as a function of crank angle and volume distribution at TDC (pie chart). At TDC, the core zone accounts for 30% of the dead volume, whereas the crevice zone accounts for 1.5%.

It was also proven that the MZM reproduced the methane conversion found experimentally in our previous work [10] within ±1.9%.

A representative natural gas is the fuel in this work, and it consist of 90% methane (CH_4), 9% ethane (C_2H_6), and 1% propane (C_3H_8). To compute the chemical kinetics of DME (CH_3OCH_3) and ozone (O_3), the Burke mechanism [20] for C1-C3 species is extended by the Zhao sub-mechanism [21] for ozone kinetics.

Table 1 presents the investigated engine properties and operation parameters. The equivalence ratio is varied between 1.5 and 2.5 and all other conditions remain constant. For the calculation of the equivalence ratio the additives are considered, and the amount of air is adjusted accordingly.

The fuel conversion X_i, product yields Y_i, and product selectivities S_i are evaluated to assess the influence of the additive choice on the chemical output of the polygeneration system. In the corresponding definitions Eqs. (6), (9), and (10), the stoichiometric coefficient, the entering molar flows, and the exiting molar flows are denoted as ν_i, $\dot{n}_i'$, and $\dot{n}_i''$, respectively. The total fuel conversion X_t in Eq. (8) considers the conversion of all fuel and additive species, weighted according to their entering mole fractions x_i' Eq. (7) in the fuel-additive mixture.

$$X_i = 1 - \left(\frac{\dot{n}_i''}{\dot{n}_i'} \right) \tag{6}$$

Table 1. Engine properties and operation parameters.

Description		Value	Unit
Rotational speed	n	1500	1/min
Compression ratio	ε	20	–
Bore	d	65	mm
Stroke	s	100	mm
No. of cylinders	Z	4	–
Displacement	D	1.327	cm^3
Equivalence ratio	Φ	1.5–2.5	–
Intake temperature	T_{in}	50	°C
Intake pressure	p_{in}	1	bar
Coolant temperature	T_C	100	°C
Th. conductivity wall	λ_W	53	W/(m K)
Convection coeff. coolant	α_c	3000	W/(m^2 K)

$$x_t^{'} = \sum\left(\frac{\dot{n}_i^{'}}{\sum \dot{n}_i^{'}}\right) = \sum x_i^{'} \tag{7}$$

$$X_t = \sum\left(x_i^{'} \bullet X_i\right) \tag{8}$$

$$Y_i = \frac{\dot{n}_i^{''} - \dot{n}_i^{'}}{\dot{n}_i^{'} \bullet x_t^{'} \bullet \nu_i} \tag{9}$$

$$S_i = \frac{Y_i}{X_t} \tag{10}$$

To evaluate the influence of the additive production on the exergetic efficiency, the HCCI engine is embedded in a system which also includes the additive production: the ozone generator and a black box model of the DME production process. Figure 2 displays a flow diagram of those three systems *add*, *poly*, and *sys*, their interconnections, and their corresponding exergy flows.

The exergetic efficiency ε_{add} of the DME production process ε_{DME} is estimated as 43.5% according to Zhang et al. [13] and the exergetic efficiency of the ozone generator ε_{ozone} is calculated within the Python model Eq. (11).

$$\varepsilon_{add} = \left.\frac{\dot{E}_{add}}{\dot{E}_{in,add}}\right|_{add=DME,ozone} \tag{11}$$

The ozone generator is supplied with air and power and provides a mixture of air and ozone. The power supply, the incoming air mass flow, and the ozone concentration in the output gas are taken from the data sheets of the Fujian Newland Entech Company [22] to calculate the exergy flows $\dot{E}$.

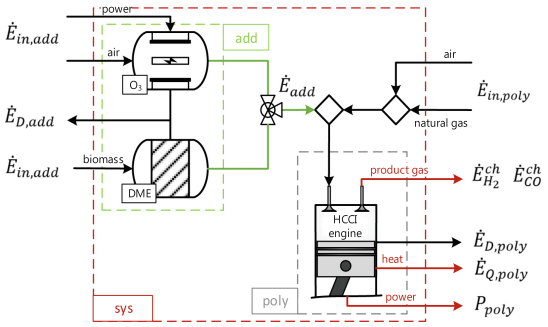

Fig. 2. Process flow diagram of the system sys, divided into two subsystems *add* and *poly*. The HCCI engine is supplied with either ozone or DME as additive.

To compare the exergy-share of DME and ozone, the exergy input ratio ε^*_{add} is defined as the ratio of the exergy flow of the additive to the total exergy flow of the engine input Eq. (12).

$$\varepsilon^*_{add} = \frac{\dot{E}_{add}}{\dot{E}_{in,poly} + \dot{E}_{add}} \tag{12}$$

Furthermore, the exergetic efficiency of the HCCI engine ε^A_{poly} and of the overall system ε^A_{sys} are defined according to Eqs. (13) and (14).

$$\varepsilon^A_{poly} = 1 - \frac{\dot{E}_{D,poly}}{\dot{E}_{in,poly} + \dot{E}_{add}} \tag{13}$$

$$\varepsilon^A_{sys} = 1 - \frac{\dot{E}_{D,poly} + \dot{E}_{D,add}}{\dot{E}_{in,poly} + \frac{\dot{E}_{add}}{\varepsilon_{add}}} \tag{14}$$

The exergy destruction $\dot{E}_D$ in the HCCI engine is estimated with the Gouy-Stodola theorem Eq. (15), the irreversible entropy production rate ($\dot{S}_{irr,poly}$) is calculated using the second law of thermodynamics.

$$\dot{E}_{D,poly} = T_{env} \bullet \dot{S}_{irr,poly} \tag{15}$$

Without full fuel conversion, the aforementioned efficiencies must be evaluated critically, since, as an extreme, the evaluated efficiency would be 100%, if no conversion takes place, which is not aimed. To assess the conversion to the wanted products only, a second definition for the exergetic efficiency is introduced for *poly* Eq. (16) and for *sys* Eq. (17), denoted with the superscript *B*.

$$\varepsilon^B_{poly} = \frac{\dot{E}^{ch}_{H_2} + \dot{E}^{ch}_{CO} + P_{poly} + \dot{E}_{Q,poly}}{\dot{E}_{in,poly} + \dot{E}_{add}} \tag{16}$$

$$\varepsilon^B_{sys} = \frac{\dot{E}^{ch}_{H_2} + \dot{E}^{ch}_{CO} + P_{poly} + \dot{E}_{Q,poly}}{\dot{E}_{in,poly} + \frac{\dot{E}_{add}}{\varepsilon_{add}}} \tag{17}$$

Here, only useful exergy stream outputs are considered: the chemical exergy flow of synthesis gas $\dot{E}^{ch}_{H_2}$ and $\dot{E}^{ch}_{CO}$, the power output P_{poly}, and the exergy flow of the heat transferred to the cooling water $\dot{E}_{Q,poly}$. Species that are not converted towards synthesis gas are thus neglected. Both definitions have advantages and disadvantages, since the second definition now neglects the possibility to re-use the unconverted educts in a following cycle. As a compromise, both will be shown.

3 Results and Discussion

First, the necessary amounts of ozone and DME for a stable combustion phasing of 7.4 ± 0.2 °CA after top dead center (°CA aTDC), using the SZM, are evaluated and compared. An ignition shortly after reaching top dead center is most favorable, the sensitivity of the combustion phasing on the exact amount of additive was investigated systematically by varying the additive amounts by ±20% at $\phi = 1.9$. The reference case for ozone represents the amount of ozone that was needed in the work of Schröder et al. [10] to substitute DME completely by ozone.

Second, these amounts are reduced or increased when reducing or increasing ϕ, respectively, and the equivalence ratio dependent product selectivities and exergetic efficiencies are discussed. All single-zone model results shown in this chapter are an average of four consecutive engine cycles. The multi-zone model results are taken from the fourth cycle.

Figure 3 illustrates the pressure traces for the DME and the ozone case at $\phi = 1.9$.

The relatively high compression ratio of 20 leads to maximum pressures of 53 bar and 59 bar before, and 174 bar and 167 bar after ignition, for DME and ozone, respectively. A similar CA50 is obtained with about 11 times less ozone compared to DME in the total mixture. In contrast to DME, ozone does not increase the molar heat capacity of the mixture and supplies radicals at lower temperatures and thus earlier crank angles. Because of the lower heat capacity, the temperature and pressure increase during the compression stroke is higher and less additive is needed. Figure 3 also indicates that small amounts of ozone shift the combustion phasing noticeably stronger, although the relative increase is stronger for DME: to shift the combustion phasing by one crank angle degree (considering the black cases as reference), additional 1.3% or rather 283 ppm DME must be added, whereas 2.5% or 50 ppm additional ozone is needed.

For DME, a small combustion phasing range is found, in which the ignition is unstable and only every second cycle ignites after intermediate species, such as formaldehyde and hydrogen peroxide, from the previous cycle are accumulated, which will be discussed later in this chapter. This effect is seen for the condition where the DME amount of the reference case is reduced by 4.5% or 950 ppm, marked in red in Fig. 3a. A pressure increase is noticeable, but the combustion phasing is very late, and the averaged pressure trace is not smooth, because every cycle differs.

The kinetic effects of ozone and DME on fuel-rich HCCI engine operated with neat methane was analyzed in our previous work [10]. We found that ozone decomposes very early and is completely converted at −40 °CA. Its decomposition yields atomic and molecular oxygen, the atoms react with methane, initiating the conversion. Furthermore, a buffer molecule was found to be important, previously: methyl hydroperoxide

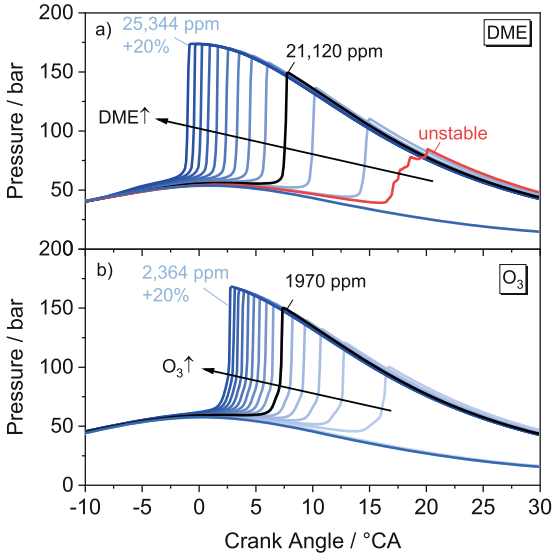

Fig. 3. Averaged pressure traces (SZM, four consecutive cycles) as a function of crank angle and additive amount in the total mixture for a) DME and b) ozone at $\phi = 1.9$. The reference additive amount (black line) is varied by $\pm 20\%$ (blue lines). For DME, an unstable ignition is found for the second lowest DME amount (red line).

(CH_3OOH). This relatively unstable molecule is formed for a brief period and increases the OH radical concentration later, due to decomposition at higher temperatures after further compression. Thus, it promotes the conversion of methane and the formation of formaldehyde (CH_2O) and hydrogen peroxide (H_2O_2), which are crucial precursors for methane ignition.

On the basis of these findings, the following section deals with the influence of the additional ethane and propane in natural gas mixtures on the intermediate species and the interaction with ozone. In this work, the engine is operated at higher rotational speed (+905 min^{-1}), higher compression ratio (+10) and lower intake temperature (−100 °C) compared to [10] in order to investigate conditions for the subsequent exergetic analysis, which are nearer to nowadays' engine parameters. This leads to a higher cylinder charge and shorter residence times.

In Fig. 4 two operating conditions are compared: the ozone reference case with 1970 ppm ozone in the total mixture (black line in Fig. 4b) and the ozone mixture with 1570 ppm ozone (−20%, dashed lines), the latter condition does not ignite (flat line in Fig. 4b).

Due to the 2.5 times shorter residence time and the lower intake temperature compared to the work of Schröder et al. [10], ozone is barely decomposed at −40 °CA. However, the higher compression ratio leads to a steeper temperature increase and thus ozone decomposition starts shortly after −40 °CA and is complete at −25 °CA. This applies for both cases and thus both ozone amounts. As a result, CH_3OOH, CH_2O and H_2O_2 are formed as described for the methane case before, but also ethyl hydroperoxide

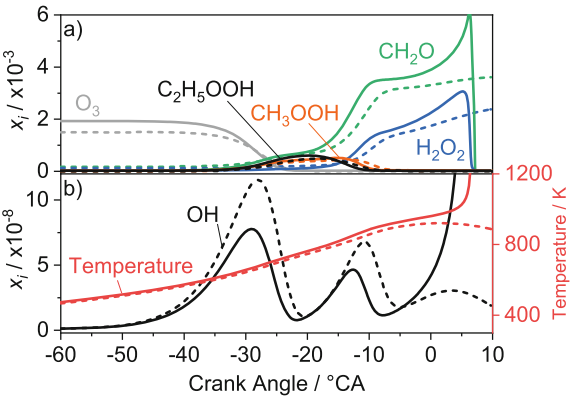

Fig. 4. Intermediate species mole fractions and in-cylinder temperature as a function of crank angle at $\phi = 1.9$ (SZM). Solid lines: 1970 ppm ozone cause ignition; dashed lines: 1570 ppm ozone (−20%) is insufficient for ignition. a) Illustrates ozone and the most important intermediate species, b) shows the in-cylinder temperature and OH radical formation.

(C2H5OOH). If the ozone amount is too low (dashed lines), CH_2O and H_2O_2 are accumulated in each cycle, the OH formation is increased, and the formation of CH_3OOH is comparable. OH radicals are formed in this first step by H-abstraction from the natural gas components, which react with oxygen atoms from the ozone decomposition. The OH radicals are then mainly reacting with the natural gas constituents, leading to a peak. Nevertheless, the second OH peak, which results from CH_3OOH decomposition to CH_3O and OH, is shifted by 2 °CA, because the temperature increases slightly slower. This leads to the effect that the expansion after reaching top dead center quenches the reactions and prevents the ignition of the mixture, illustrated by low OH radical amounts and no CH_2O or H_2O_2 conversion. However, the OH radical mole fraction is slightly higher in the non-igniting case, since CH_2O and H_2O_2 are accumulated, which lead to additional OH radical formation. Nevertheless, this effect is not sufficient for achieving ignition.

In Fig. 5, the case with 1970 ppm ozone which leads to ignition for natural gas, is compared to a methane case with the same ozone amount.

It is seen that the natural gas mixture starts to ignite, while methane is not converted yet. In the methane case the CH_3OOH formation shows a distinctive maximum at −22 °CA, whereas in the natural gas case, the formation is reduced at that point, and the maximum is found later at −14.4 °CA. In addition, ethene and propene are formed from twostep H abstractions from ethane and propane by OH radicals and ethyl hydroperoxide, as well as ethene and propene are formed as further buffer molecules. Kaczmarek et al. [12] showed that ethene and propene are typical intermediate species for the fuel-rich combustion of natural gas and that ethane and propane do not influence the CH_3OOH formation. This leads to a lower CH_3OOH mole fraction compared to the methane case, but due to the exothermal H-abstraction of ethane and propane, which leads to an intermediate C2H5OOH formation, the in-cylinder temperature and OH radical concentration are high enough for ignition. The initial ethane and propane mole

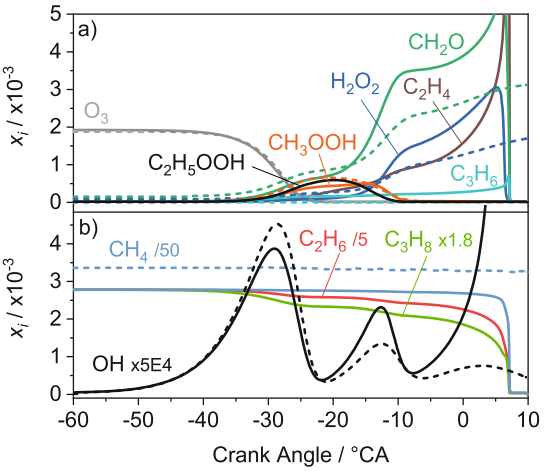

Fig. 5. Intermediate species mole fractions as a function of crank angle at $\phi = 1.9$ (SZM). Solid lines: natural gas; dashed lines: methane. a) Illustrates ozone and the most important intermediate species, b) shows the fuel conversion and OH radical formation.

fractions in the mixture correspond to 14,180 ppm and 1,580 ppm, respectively. If neat methane is to be ignited instead, these additives have to be replaced by only 640 ppm ozone, which emphasizes the effectiveness of ozone as an ignition promoter. The product yields are not affected by combustion phasing and are thus not further discussed here.

In the subsequent section, the necessary ozone and DME amounts for the equivalence ratio range of 1.5 to 2.5, to achieve ignition at CA50 = 6.5 ± 0.6 °CA, and the influence on the exergetic efficiencies are discussed. Figure 6a shows the necessary mole and mass fractions of DME and ozone as a function of equivalence ratio. Figure 6b illustrates the resulting exergy contribution of the additive to the exergy entering the engine ε^*_{add} and the efficiency of the additive production ε_{add}.

With increasing equivalence ratio, the additive mole and mass fractions needed for ignition increase for both additives. However, the DME-related gradients are larger: 1.0 mol-%/ϕ for DME and only 0.065 mol-%/ϕ for ozone. Up to 2.7 mol-% and 4.5 mass-% of DME in the total mixture are needed. This is about 9.9 to 11.6 times more compared to the ozone case, increasing with ϕ. The difference of the exergy ratios ε^*_{add} are even higher, as Fig. 6b illustrates. DME contributes 21% to the exergy input, whereas ozone is only accountable for a negligible contribution of 0.2%. On the contrary, the calculated exergetic efficiency of the ozone generator is poor with a rather constant value of 5.5%. At $\phi = 2.5$, for instance, 4.28 kW of electrical energy must be supplied to generate an ozone mass flow of 0.26 kg/h. The multi-zone model predicts similar figures for the DME case, for which it was validated. On the contrary, when the additive is switched from DME to ozone, much higher ozone amounts or higher intake temperatures are needed compared to the single-zone model. In Fig. 6, the multi-zone model results with ozone are obtained with an intake temperature of 100 °C, which is 50 °C higher than in the SZM case; this leads to an ignition with the same amount of ozone as in the single-zone model. Although ozone decomposes early in the compression stroke, it needs about 38°

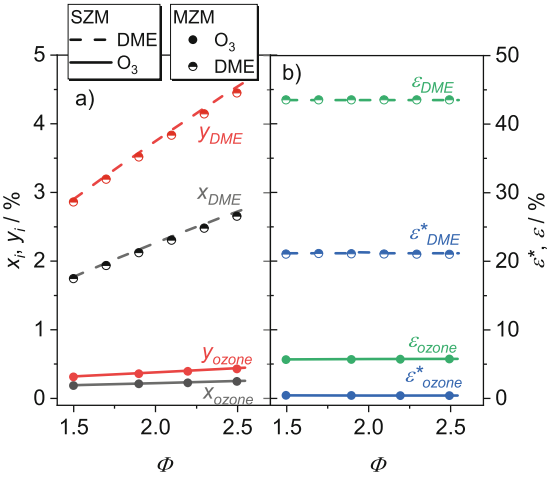

Fig. 6. a) Intake additive mole fractions x_i in black and mass fractions y_i in red, and b) intake exergy ratio ε^*_{add} and exergetic efficiency of the additive production ε_{add} as a function of equivalence ratio at CA50 = 6.5 ± 0.6 °CA (solid lines: ozone, dashed lines: DME; filled symbols: ozone multi-zone model with T_{in} = 100 °C (+50 °C), semi-filled symbols: DME multi-zone model).

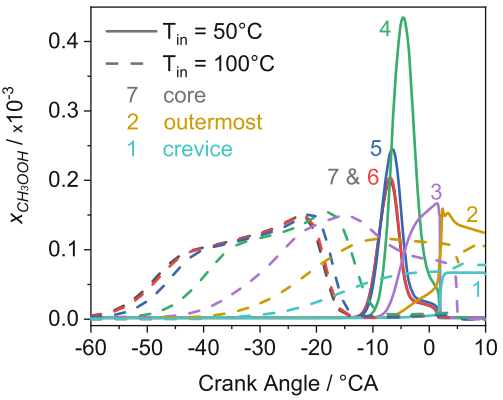

Fig. 7. Methyl hydroperoxide (CH_3OOH) mole fraction as a function of crank angle for all seven zones of the multi-zone model (ϕ = 1.9). Solid lines: intake temperature of 50 °C, no ignition. Dashed lines: intake temperature of 100 °C, ignition.

crank angle for full decomposition in the core zone (ϕ = 1.9, T_{in} = 50 °C). This leads to a relatively late CH_3OOH formation and decomposition compared to the single-zone model. In the single-zone model, as shown in Fig. 4a and Fig. 5a, CH_3OOH is completely converted at −8 °CA. By contrast, in the multi-zone model, CH_3OOH is converted in the four innermost zones until +2 °CA, and no ignition is achieved. With an increased intake temperature of 100 °C, CH_3OOH is converted again at −8 °CA, comparable to the single-zone model, and the mixture ignites. This is illustrated in Fig. 7.

In contrast to ozone, DME converts late in the compression stroke and in the core zone: it is converted nearly twice as fast, which makes DME less sensitive on the heat and mass transfer from the core zone to its adjacent zones. This shows that due the complexity of the heat and mass transfer within the multi-zone model, this model must be validated against ozone measurements explicitly and investigated further in future work.

However, as seen from Fig. 8, the system's resulting exergetic efficiency decrease is minor compared to the DME case. In the figure, a comparison of the single-zone and multi-zone model is also included.

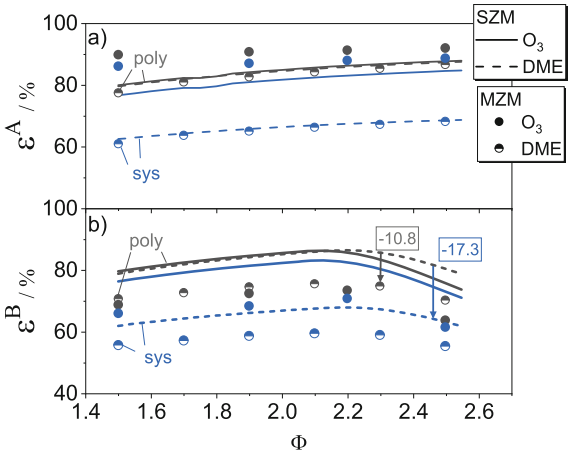

Fig. 8. Exergetic efficiency of the HCCI engine (*poly*, grey) and the entire system (*sys*, blue) as a function of equivalence ratio ϕ at CA50 $= 6.5 \pm 0.6$ °CA (solid lines: ozone, dashed lines: DME; filled symbols: ozone multi-zone model with $T_{in} = 100$ °C (+50 °C), semi-filled symbols: DME multi-zone model). Top: definition A, bottom: definition B.

The exergetic efficiency of the HCCI engine (*poly*) reaches a value of 87.5%, regardless of which additive is used. Figure 8a also indicates that when the conversion is not considered in the efficiency definition, there is no distinctive difference between the SZM and MZM results. If the whole system is regarded, including the production efficiency of the additive, and not only the engine, further differences are recognized. The strong efficiency reduction by the DME production by up to 17.3 percentage points at $\phi = 2.5$ (Fig. 8b, blue arrow) is remarkable, whereas the ozone production with the quite inefficient generator only leads to a reduction by 2.7 percentage points.

When the efficiency is defined only with the intended products, as done in definition B, Fig. 8b results from it. The efficiencies of ozone and DME still reach high values of 86.1% and 86.3%, respectively, but at lower equivalence ratios. At higher equivalence ratios, methane remains in the product gases, leading to a drop. The maximum efficiency for DME addition is slightly shifted to higher equivalence ratios compared to ozone addition: 2.2 compared to 2.15 in the ozone case.

The efficiency reduction, when the efficiency of additive production is considered (*sys*), is noticeable as well. In the DME case, the maximum efficiency decreases by 18.6

percentage points to 67.7%. With ozone there is a smaller reduction by 3.3 percentage points to 82.8%.

At $\phi = 2.2$ the conversion starts decreasing with decreasing amount of oxygen and thus the efficiency decreases as well. At $\phi = 2.3$, the efficiency of the HCCI engine (*poly*) calculated with the multi-zone model is up to 10.8 percentage points lower than those predicted by the single zone model (Fig. 8b, grey arrow). This is mainly an effect of the reduced conversion due to colder regions in the cylinder, e.g. crevice zones and zones adjoining the cylinder walls. With reduced conversion, the efficiency decreases since less chemical energy of the fuel is converted to work, heat, and synthesis gas.

In Fig. 9, the conversions predicted by the single-zone model and multi-zone model are compared.

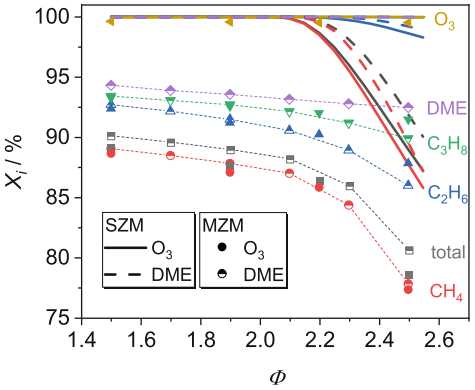

Fig. 9. Fuel and DME conversions as a function of equivalence ratio at CA50 = 6.5 ± 0.6 °CA (solid lines: ozone, dashed lines: DME, filled symbols: ozone multi-zone model with $T_{in} = 100$ °C (+50 °C), semi-filled symbols: DME multi-zone model).

In the single-zone model, propane and DME are always completely converted, whereas the ethane conversion decreases slightly at equivalence ratios above 2.2. The methane conversion is the lowest, so that the total conversion is 90.0% for DME and 87.2% for ozone at $\phi = 2.5$. The natural gas/DME mixture is more reactive at TDC, since DME is not fully converted until ignition occurs. This leads to a slightly higher overall fuel conversion compared to ozone and thus higher exergetic efficiencies at higher equivalence ratios, as seen in Fig. 8b.

The results of the multi-zone model shall be compared further to the single-zone-model. The multi-zone model predicts up to 12 percentage points smaller total conversions; values of 80.6% to 90.1% are estimated and thus the efficiencies are reduced. DME is converted by 94.3% to 92.4%, decreasing with ϕ – mainly because of the unreactive crevice zone, which, for example at $\phi = 1.9$, contains 3.5% to 9% of the total cylinder mass during combustion. This mass stems from mass transfers from outer, cooler zones when the inner zones ignite and induce a pressure increase. On the contrary, ozone is always converted completely, as emphasized before. The MZM calculations with ozone provide no additional insights since the outcome does not differ significantly from the single zone model results and are not further discussed in the following.

The efficiency reduction for DME addition at $\phi = 2.5$ is illustrated in more detail in Fig. 10, where the exergy stream outputs for the SZM and MZM are compared.

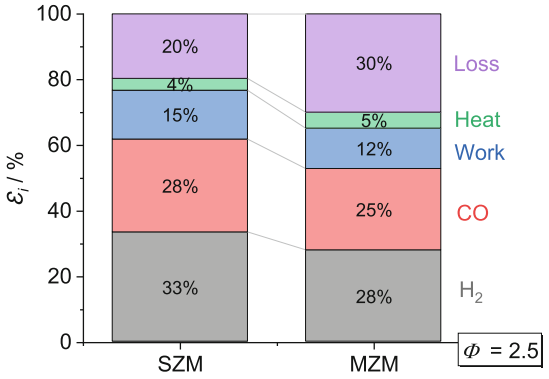

Fig. 10. Segmentation of the system's exergy stream outputs; comparison of the single zone model on the left and the multi-zone model on the right at $\phi = 2.5$ in the DME case.

The lower conversion in the MZM leads correspondingly to lower heat, work, and synthesis gas exergy streams in the system output. Nevertheless, the changes are quite uniform for the different useful outputs.

To determine promising operating conditions, it is also imperative to evaluate the equivalence ratio dependent product selectivities and compare them for both additives. In Fig. 11, the equivalence ratio dependence of the selectivities of CO, CO_2, H_2, H_2O, C_2H_2 and C_2H_4 are shown, again from both models. The main finding is that the predicted selectivities mainly depend on the equivalence ratio but only to a minor extent on the additive or the model used.

The acetylene (C_2H_2) and ethene (C_2H_4) selectivities reach 1.4% and 2.6% at the maximum investigated equivalence ratio of 2.5. Higher selectivites are expected at equivalence ratios of 5 and higher [23], but since synthesis gas is the target chemical here, these regions are not further examined. The synthesis gas selectivites increase with increasing equivalence ratio and reach a maximum at the equivalence ratio, where the highest efficiencies were found. Again, the maximum selectivities in the DME case are shifted slightly to higher equivalence ratios, compared to ozone. The maximum achievable selectivities of CO and H_2 are 88.4% and 66.5%, respectively. The MZM predicts slightly smaller synthesis gas selectivities and instead a small increase of the water selectivity. In comparison with methane, the natural gas selectivities do not differ noticeably for any investigated case. In practice, the natural gas composition does thus not influence the outcome of the process and must not be considered, when at least 90% of the natural gas consists of methane. However, for combustion control it is surely important to consider natural gas composition changes, since ignition is sensitive on this composition. Therefore, for combustion control, the additive mass flow must be adjusted on the same time-scale as the natural gas composition varies.

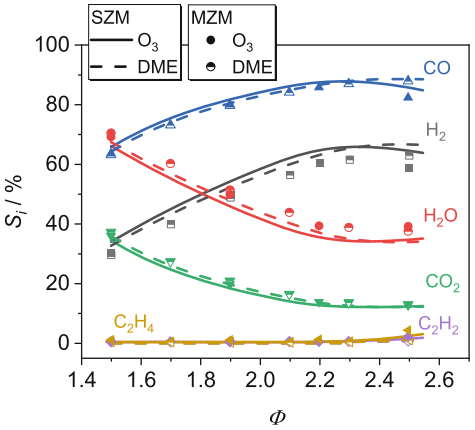

Fig. 11. Selectivities of the most important product gas species as a function of equivalence ratio ϕ at CA50 $= 6.5 \pm 0.6$ °CA (solid lines: ozone, dashed lines: DME, filled symbols: ozone multi-zone model with $T_{in} = 100$ °C (+50 °C), semi-filled symbols: DME multi-zone model).

Finally, the decision about the most favorable additive for polygeneration in fuel-rich HCCI engines is not based on the product gas composition, but on the effort in producing the additive and its fuel conversion enhancement properties.

4 Conclusions

Fuel-rich HCCI engines for polygeneration of work, heat, and synthesis gas can be operated with natural gas with the help of additives such as ozone or DME. In this work, the influence of ozone on natural gas ignition and the exergy input of DME and ozone were investigated theoretically, and the influence of the additive production on the exergetic efficiency was evaluated.

The single-zone model results showed that natural gas is much more reactive than methane. Ethane and propane convert partially in the compression stroke and lead to ethene, propene, and OH radicals. However, the ethane and propane conversions do not favor, but slightly reduce the formation of methyl hydroperoxide, which is an important buffer molecule for fuel-rich methane ignition. Instead, ethyl hydroperoxide is intermediately formed as a second buffer molecule. If the same ignition timing shall be achieved with neat methane, ethane and propane can be substituted by only 640 ppm additional ozone, which emphasizes the efficiency of the ozone decomposition.

Compared to ozone, the necessary DME molar and mass fractions are up to 11 times higher, and its exergy contribution to the total mixture is even 95 times higher: DME contributes 21% to the exergy input of the engine, whereas 1700 ppm ozone only contribute 0.2%.

The exergetic efficiency of the ozone generator was determined and reached small values of 5.5%, but since ozone is used in small quantities the system's efficiency declines by only 3.3 percentage points and reasonable values of 82.8% are possible. The DME production reduces the system's efficiency by unfavorable 17 percentage points. The

multi-zone model results show that the efficiency is strongly dependent on the fuel conversion and thus non-converted fuel should be recycled within the polygeneration system to maintain high efficiencies – especially at very fuel rich conditions.

The single-zone model predicted the product selectivities accurately and provided helpful species profiles for kinetic analyses. Additionally, if the exergetic efficiency is calculated with the Gouy-Stodola theorem, the resulting exergetic efficiencies only differed about 1 percentage point from the ones calculated with the multi-zone model. If the fuel conversion and the exergetic efficiency considering the conversion must be predicted accurately, the multi-zone model is much more suitable. The fuel conversion calculated by the multi-zone model matched our experimental values by $\pm 1.9\%$ and the exergetic efficiency was found to be 10.8 percentage points lower in the DME case. Since the multi-zone model has not been validated against ozone experiments so far, these results were obtained with a 50 °C higher intake temperature. Therefore, those conditions will be used for validation of the multi-zone model against natural gas/ozone experiments in a future work.

To conclude, ozone is a more favorable additive compared to DME – not only based on the necessary mass flows but on exergetic efficiency as well. These results encourage profound investigations of ozone kinetics for fuel-rich combustion technologies that require reactive fuel additives.

Acknowledgments. This research was funded by Deutsche Forschungsgemeinschaft (DFG), grant number 229243862 (AT24/13–3) within the framework of the DFG research unit FOR 1993 'Multi-functional conversion of chemical species and energy'. The authors gratefully acknowledge the DFG for the financial support.

References

1. Karim, G.A., Wierzba, I.: The production of hydrogen through the uncatalyzed partial oxidation of methane in an internal combustion engine. Int. J. Hydrogen Energy **33**, 2105–2110 (2008). https://doi.org/10.1016/j.ijhydene.2008.01.051
2. Lim, E.G., et al.: The engine reformer: Syngas production in an engine for compact gas-to-liquids synthesis. Can. J. Chem. Eng. **94**, 623–635 (2016). https://doi.org/10.1002/cjce.22443
3. Banke, K., Hegner, R., Schröder, D., Schulz, C., Atakan, B., Kaiser, S.A.: Power and syngas production from partial oxidation of fuel-rich methane/DME mixtures in an HCCI engine. Fuel **243**, 97–103 (2019). https://doi.org/10.1016/j.fuel.2019.01.076
4. Wiemann, S., Hegner, R., Atakan, B., Schulz, C., Kaiser, S.A.: Combined production of power and syngas in an internal combustion engine – experiments and simulations in SI and HCCI mode. Fuel **215**, 40–45 (2018). https://doi.org/10.1016/j.fuel.2017.11.002
5. Kaczmarek, D., Atakan, B., Kasper, T.: Investigation of the partial oxidation of methane/n-heptane-mixtures and the interaction of methane and n-heptane under ultra-rich conditions. Combust. Flame **205**, 345–357 (2019). https://doi.org/10.1016/j.combustflame.2019.04.005
6. Hegner, R., Werler, M., Schießl, R., Maas, U., Atakan, B.: Fuel-rich HCCI engines as chemical reactors for polygeneration: a modeling and experimental study on product species and thermodynamics. Energy Fuels **31**, 14079–14088 (2017). https://doi.org/10.1021/acs.energyfuels.7b02150

7. Kebriaei, M., HalvaeiNiasar, A., Ketabi, A.: A new pulsed power generator topology for corona discharge. In: 2016 7th Power Electronics and Drive Systems Technologies Conference (PEDSTC), 16−18 Feb 2016, pp. 577–581. IEEE, Tehran, Iran (2016)
8. Keum, S., Kuo, T.W.: Damköhler number analysis on the effect of ozone on auto-ignition and flame propagation in internal combustion engines. In: Volume 1: Large Bore Engines; Fuels; Advanced Combustion, 4 November 2018, V001T03A002. ASME, San Diego, California (2018)
9. Sayssouk, S., Nelson-Gruel, D., Caillol, C., Higelin, P., Chamaillard, Y.: Towards control of HCCI combustion by ozone addition: a mathematical approach to estimate combustion parameters. In: IFAC-PapersOnLine, vol. 49, pp. 361–368 (2016). https://doi.org/10.1016/j.ifacol.2016.08.054
10. Schröder, D., Banke, K., Kaiser, S.A., Atakan, B.: The kinetics of methane ignition in fuel-rich HCCI engines: DME replacement by ozone. In: Proceedings of the Combustion Institute, vol. 38, pp. 5567−5574 (2020).https://doi.org/10.1016/j.proci.2020.05.046
11. Duan, X., et al.: Effects of natural gas composition and compression ratio on the thermodynamic and combustion characteristics of a heavy-duty lean-burn SI engine fueled with liquefied natural gas. Fuel **254**, 115733 (2019). https://doi.org/10.1016/j.fuel.2019.115733
12. Kaczmarek, D., et al.: Plug-flow reactor and shock-tube study of the oxidation of very fuel-rich natural gas/DME/O2 mixtures. Combust. Flame **225**, 86–103 (2021). https://doi.org/10.1016/j.combustflame.2020.10.004
13. Zhang, X., Solli, C., Hertwich, E.G., Tian, X., Zhang, S.: Exergy analysis of the process for dimethyl ether production through biomass steam gasification. Ind. Eng. Chem. Res. **48**, 10976–10985 (2009). https://doi.org/10.1021/ie900199e
14. Goodwin, D.G., Speth, R.L., Moffat, H.K., Weber, B.W.: Cantera: an object-oriented software toolkit for chemical kinetics, thermodynamics, and transport processes (2021). https://www.cantera.org. Version 2.4.0
15. Komninos, N.P., Rakopoulos, C.D.: Heat transfer in HCCI phenomenological simulation models: a review. Appl. Energy **181**, 179–209 (2016). https://doi.org/10.1016/j.apenergy.2016.08.061
16. Komninos, N.P., Hountalas, D.T., Kouremenos, D.A.: Development of a new multi-zone model for the description of physical processes in HCCI engines. In: SAE Technical Paper 2004-01-0562. https://doi.org/10.4271/2004-01-0562
17. Yang, J., Martin, J.K.: Approximate solution—one-dimensional energy equation for transient, compressible, low mach number turbulent boundary layer flows. J. Heat Transf. **111**, 619–624 (1989). https://doi.org/10.1115/1.3250727
18. Woschni, G.: A universally applicable equation for the instantaneous heat transfer coefficient in the internal combustion engine. In: SAE Technical Paper 670931. https://doi.org/10.4271/670931
19. Chang, J., et al.: New heat transfer correlation for an HCCI engine derived from measurements of instantaneous surface heat flux. In: SAE Technical Paper 2004-01-2996. https://doi.org/10.4271/2004-01-2996
20. Burke, U., et al.: An ignition delay and kinetic modeling study of methane, dimethyl ether, and their mixtures at high pressures. Combust. Flame **162**, 315–330 (2015). https://doi.org/10.1016/j.combustflame.2014.08.014
21. Zhao, H., Yang, X., Ju, Y.: Kinetic studies of ozone assisted low temperature oxidation of dimethyl ether in a flow reactor using molecular-beam mass spectrometry. Combust. Flame **173**, 187–194 (2016). https://doi.org/10.1016/j.combustflame.2016.08.008

22. Fujian Newland Entech Company, Ozone Portfolio (2017). https://newlandentecheurope.com/wp-content/uploads/2017/06/Newland-EnTech-Europe_Ozone.pdf. Accessed 24 Feb 2021
23. Atakan, B., et al.: Flexible energy conversion and storage via high-temperature gas-phase reactions: The piston engine as a polygeneration reactor. Renew. Sustain. Energy Rev. **133**, 110264 (2020). https://doi.org/10.1016/j.rser.2020.110264